

1 **A Library of Early Cambrian Chemostratigraphic Correlations from a Reproducible**  
2 **Algorithm**

3 Carling C. Hay<sup>1\*</sup>, Jessica R. Creveling<sup>2</sup>, Cedric J. Hagen<sup>2</sup>, Adam C. Maloof<sup>3</sup>, Peter Huybers<sup>4</sup>

4 <sup>1</sup>Earth and Environmental Sciences, Boston College, Chestnut Hill, MA 02467, USA

5 <sup>2</sup>College of Earth, Ocean, and Atmospheric Sciences, Oregon State University, Corvallis, OR 97330, USA

6 <sup>3</sup>Department of Geosciences, Princeton University, Princeton, NJ 08544, USA

7 <sup>4</sup>Earth and Planetary Sciences, Harvard University, Cambridge, MA 02138, USA

8 *\*Corresponding author*

9

10 **Contents:**

11

12 *Alignment Path and the Cost Matrix* 2

13 *Additional Alignments for S11* 3

14 *Relative and Absolute Sediment Accumulation*  
15 *Rates for S3 and S11* 5

16

17

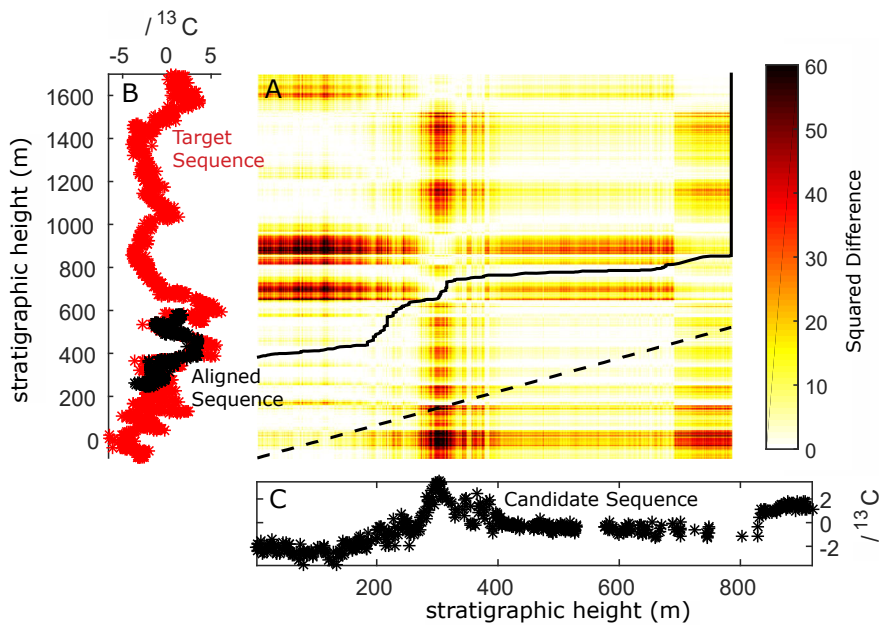
18 *Matlab Code for Methodology*

19 2019175\_Matlab Code.txt

20

21 **Alignment Paths and the Cost Matrix**

22 The alignments shown in the main text are determined by finding the minimum cumulative  
23 squared difference path through the cost matrix. Figure DR1A shows an example squared  
24 distance cost matrix for the alignment of S3 with the target sequence (S16). The alignment path  
25 is obtained for an edge parameter value of 0.1 and a  $g$  value of 1. The target sequence (Fig.  
26 DR1B, red line) and original candidate sequence (Fig. DR1C) are plotted along the vertical and  
27 horizontal axes, respectively. A single cost matrix value at row  $i$  and column  $j$  is found by  
28 computing the squared difference between the target data at row  $i$  and the candidate data in  
29 column  $j$ . Dark red colors indicate large squared differences between the data points while white  
30 colors correspond to identical or nearly identical data in both time series. The black dashed line  
31 shown in the cost matrix represents the diagonal path that would be taken if both sequences  
32 began at the same depth and had the same accumulation rate.



33  
34 **Figure DR1.** A) The squared difference cost function and the resulting alignment path (solid black line)  
35 for the alignment of the S3 section with the target using an edge parameter value of 0.1 and a  $g$  value of 1.  
36 The dashed line shows the path that would be taken if both time series had the same sampling and  
37 accumulation rate and if both time series were assigned the same initial depth. B) The target sequence  
38 (red) and the aligned candidate sequence. C) The original candidate time series.

39  
40  
41  
42

43 ***Additional Alignments for S11***

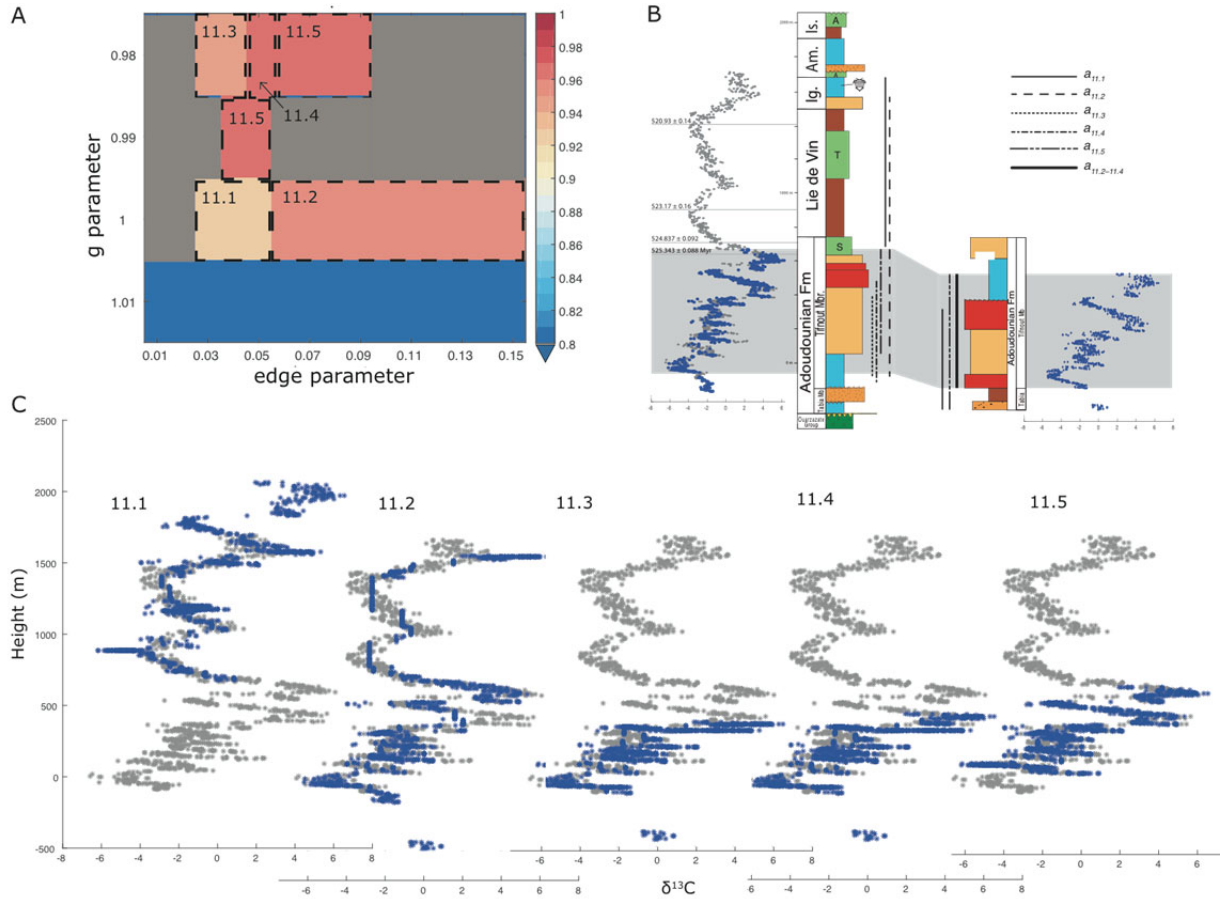
44 The alignment of S11 to S16, obtained from a lower resolution search of the edge and  $g$   
45 parameter space (Fig. DR2A), yields five distinct solutions  $a_{11.1-11.5}$  (Fig. DR2C). The related  
46 synthetic test produced a range of p-values for the average correlation coefficient for which the  
47 null hypothesis of no true correlation can be rejected in only one case (Table DR1,  $g=1$ ). Despite  
48 the high average correlation coefficients, we cannot favor an individual solution based on  
49 statistical significance alone.

50

51 Solution  $a_{11.1}$ , with a  $g$  value near 1 and edge values  $< 0.5$ , aligns S11 to the sigmoidal  $\delta^{13}\text{C}_{\text{carb}}$   
52 variation above S16 660 m and extends a subset of S11 above S16 (Fig. DR2B). This solution  
53 correlates strata assigned to the Adoudounian Formation at S11 to wholly younger  
54 lithostratigraphic units at S16 and in this regard represents a solution nearly antithetical to  
55 Maloof et al. (2010b; Fig. DR2B). Solution  $a_{11.2}$ , with a  $g$  value near 1 and edge values  $>0.5$ ,  
56 stretches S11 to span nearly the entire duration of S16 and, in doing so, imposes numerous  
57 hiatuses in S11. If physical, this would imply that strata assigned to the Adoudounian Formation  
58 at S11 partly coeval with strata assigned a younger age at S16 (Maloof et al., 2005). As such,  
59  $a_{11.1}$  and  $a_{11.2}$  find the least support in that they align non-fossiliferous lithostratigraphic units  
60 assigned to Cambrian Series 1 at S11 to fossiliferous Cambrian Series 2 units at S16 (Fig.  
61 DR2B). Thus, we do not present  $a_{11.1}$  or  $a_{11.2}$  in the library of plausible solutions in Figure 2.

62

63  $a_{11.3} - a_{11.5}$  align the same lithostratigraphic unit at S11 and S16 (Fig. DR2B), and therefore these  
64 plausible solutions are discussed in the main text and reproduced in Figure 2 of the main text.



65  
 66 **Figure DR2.** Dynamic programming alignment of S11  $\delta^{13}C_{carb}$  data (Maloof et al., 2005) to S16 (Maloof  
 67 et al., 2010a). (A) Correlation coefficients for solution sets with specified  $g$  and edge parameters. Grey  
 68 areas show parameter pairings without valid alignments (see main text). (B) Alignments  $a_{11.1}$ – $a_{11.5}$  for  
 69 parameter pairs shown in (A). S11  $\delta^{13}C$  data (blue) scaled to the stratigraphic height of S16 (grey). (C)  
 70 Lithostratigraphic correlations (see inset) implied by chemostratigraphic alignments  $a_{11.1}$ – $a_{11.5}$ .

71

72

73

74

Alignment	edge value	$g$ value	average correlation	p-value
S11 to S16	0.2	0.980	0.8635	0.850
	0.2	0.990	0.8470	0.940
	0.2	1.000	0.9355	0.013
	0.2	1.010	0.1017	0.700

79

80 **Table DR1.** Average correlation coefficients and associated p-values for the alignment of S11 to  
 81 S16 for an edge value of 0.2 and  $g$  values from 0.980–1.010.

82

83 Each solution imposes hiatuses in S11 and S16 that could imply limited temporal overlap  
84 between sections, consistent with lateral facies variation observed in the constituent subtidal to  
85 peritidal mixed carbonate–siliciclastic parasequences disrupted by synsedimentary slumping  
86 (Buggisch and Heinitz, 1984; Maloof et al., 2005). Alternatively, frequent hiatuses could be an  
87 artifact of our procedure whereby imposing hiatuses is necessary when aligning relatively  
88 contracted or extended records.

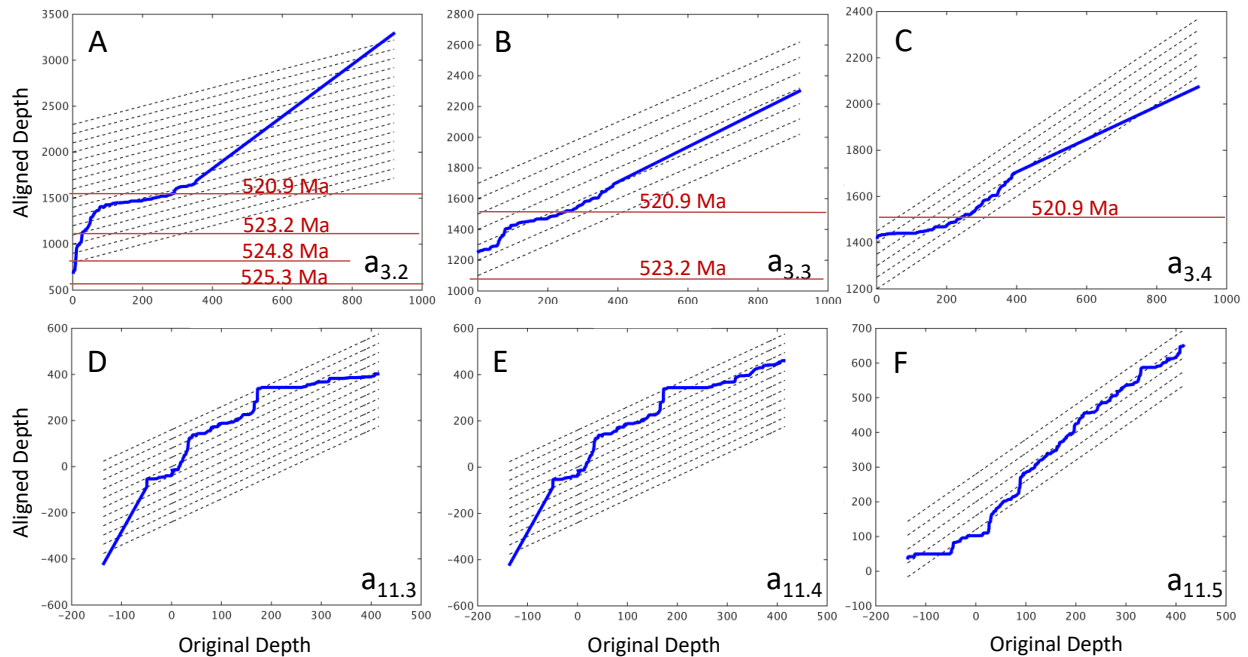
89  
90 In summary, solutions  $a_{11.3}$  and  $a_{11.4}$  correlate S11 to the oldest strata of the Adoudounian  
91 Formation at S16, however, neither predicts that S11 deposition span the entire duration of  
92 deposition of the Adoudounian Formation. By comparison,  $a_{11.5}$  implies S11 deposition both  
93 initiated and ended later, though the predicted hiatus at S16 equivalent to the deposition of the  
94 upper Tabia Member at S11 is inconsistent with the visual correlation of Maloof et al. (2010b).

95

#### 96 ***Relative and Absolute Sediment Accumulation Rates for S3 and S11***

97 To further explore the plausibility of alignment solutions, we compared the relative and absolute  
98 time history of sediment accumulation implied by alignment solutions to physical stratigraphic  
99 surfaces and/or lithologic boundaries across which one would suspect changes in sedimentation.  
100 Figure DR3 presents *relative* sediment accumulation rates between S16 and the candidate  
101 sections S3 and S11. When reading these frames (Fig. DR3A–F), a vertical trajectory for the  
102 accumulation curve requires a hiatus in the candidate section coincident with sediment  
103 accumulation at the target section (S16), whereas a horizontal trajectory indicates the converse.  
104 Between these extremes, a slope greater than 1:1 implies that the target sequence accumulated  
105 more rapidly than the candidate (‘stretching’ the candidate) while a slope less than 1:1 indicates  
106 the converse (‘squeezing’ the candidate). Note that an inflection in the relative rate of  
107 accumulation can result from a change in the rate of sediment accumulation at either the target or  
108 the candidate sequence, or both. Thus, for these plots, a change in the relative rate of  
109 accumulation corresponding to a lithological transition or lithostratigraphic boundary need not  
110 reflect the change in sedimentation rate at an individual section, but rather a new relative rate of  
111 accumulation between the target and candidate sequences as compared to that from the  
112 underlying lithology.

113



114  
115  
116  
117  
118  
119  
120

**Figure DR3.** Relative rates of sediment accumulation for the preferred alignment solutions between (A)–(C) S16 and S3 and (D)–(F) S16 and S11. Horizontal lines show the extrapolated stratigraphic height of radiometric dates (with ages in Ma; Maloof et al., 2010a).

121 Alignment solution  $a_{3.2}$  implies that below  $\sim 80$  m, S16 accumulated more rapidly than S3 and  
 122 above this depth, to the Lie De Vine–Igoudine contact (see Fig. 1b), S3 accumulated more  
 123 rapidly than S16 (Fig. DR3A). In contrast, solution  $a_{3.3}$  implies a nearly constant relative rate of  
 124 accumulation between S3 and S16 through time (Fig. DR3B), and this may lend credence to  
 125 solution  $a_{3.3}$  if such consistency reflects uniform sediment accumulation across space on a  
 126 subsiding margin. Conversely, solution  $a_{3.4}$  implies that, initially, S3 accumulated more rapidly  
 127 than S16 and subsequently transitioned to nearly equal sediment accumulation at the two locales  
 128 before culminating in more rapid deposition at S16 (Fig. DR3C).

129

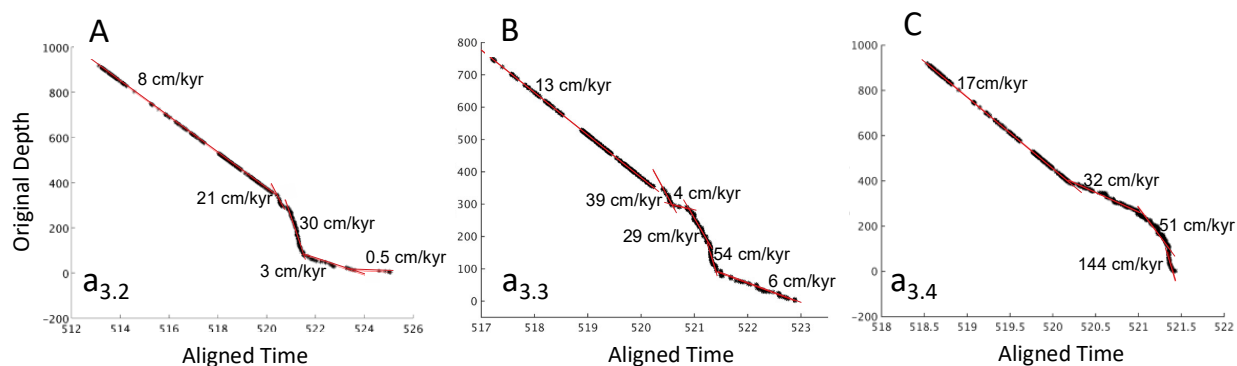
130 Relative sediment accumulation rates for alignments  $a_{11.3}$  and  $a_{11.4}$  show a similar transition from  
 131 more rapid accumulation at S16 to more rapid accumulation at S3 (Fig. DR3D,E). In contrast,  
 132 alignment  $a_{11.5}$  implies S11 accumulated at a similar rate to S16 (Fig. DR3F).

133

134 If the target section hosts radiometric dates that span the aligned stratigraphic interval, then the  
 135 time history of *absolute* sedimentation rate can be inferred (Fig. D56). To infer the time history

136 of absolute sediment accumulation rates at a candidate section, the following assumption must  
 137 hold: the target sequence must encompass a complete record of sediment deposition such that the  
 138 linear interpolation of time between any two hypothetical dates is valid. To this end, we estimate  
 139 linearly interpolated absolute sediment accumulation rates between radiometric constraints at S3  
 140 by: (1) adopting the Cambrian linear age model of Maloof et al. (2010a) for S16, (2) using a  
 141 dynamic programming alignment solution to translate the stratigraphic height of the four  
 142 radiometric datums at S16 to the corresponding meterage at S3 (see Fig. DR3C and discussion  
 143 above), and (3) dividing the total meterage between any two extrapolated dates at S3 by the age  
 144 difference. Alignments  $a_{3,2}$  and  $a_{3,3}$  produce a range of apparent sedimentation rates, from 0.5–54  
 145 cm/kyr (Fig. DR4A,B), of similar magnitude to that determined by Maloof et al. (2010b; 16–25  
 146 cm/kyr). The wider range in sedimentation rate implied by  $a_{3,4}$  results from squeezing the  
 147 lowermost 288 m of S3 into 76 m below the 520.93 Ma ash bed, yielding an average rate of 144  
 148 cm/kyr (Fig. D45C).

149  
 150  
 151



152  
 153 **Figure DR4.** Absolute rates of sediment accumulation between S16 and S3. (A)–(C) Implied  
 154 absolute sediment accumulation rates (red lines and values) for each of the three preferred  
 155 alignments of S3 to S16 assuming the linear age model of Maloof et al. (2010a; see also Fig. 2).  
 156

157  
 158 **Supplementary References**

159 Buggisch, W., and Heintz, W., 1984, Slumpfolds and other early deformations in the early Cambrian of the Western  
 160 and Central Anti-Atlas (Morocco): *Geologische Rundschau*, v. 73, p. 809–819.  
 161 Maloof, A.C., Schrag, D.P., Crowley, J.L., and Bowring, S. a., 2005, An expanded record of Early Cambrian carbon  
 162 cycling from the Anti-Atlas Margin, Morocco: *Canadian Journal of Earth Sciences*, v. 42, p. 2195–2216,  
 163 doi:10.1139/e05-062.